001. The experiment was done at the Integrated Optics Laboratory, Department of Electrical Engineering, National Taiwan University, R.O.C. The authors would like to express their appreciation to Prof. Way-Seen Wang and Jeremy C. Smith for their encouragement and helpful suggestions.

REFERENCES

1. G.K. Gopalakrishnan, C.H. Bulmer, W.K. Burns, R.K. McElhanon, and A.S. Greenblatt, 40GHz, low half-wave voltage Ti:$LiNbO_3$ intensity modulator, Electron Lett 8 (1992), 826–287.
2. D.W. Dolfi and T.R. Ranganth, 50GHz, velocity-matched broad wavelength $LiNbO_3$ modulator with multimode active section, Electron Lett 28 (1992), 1197–1198.
3. K. Kawano, T. Kitoh, O. Mitomi, T. Nozawa, and M. Yanagibashi, New travelling-wave electrode Mach-Zehnder optical modulator with 20GHz bandwidth and 4.7V driving voltage at 1.52μm wavelength, Electron Lett 25 (1989), 1382–1383.
4. K. Noguchi, K. Kawano, T. Nozawa, and T. Suzuki, A Ti:$LiNbO_3$ optical intensity modulator with more than 20GHz bandwidth and 5.2V driving voltage, IEEE Photon Technol Lett 3 (1991), 333–335.
5. K. Noguchi, O. Mitomi, K. Kawano, and M. Yanagibashi, Highly efficient 40GHz bandwidth Ti:$LiNbO_3$ optical modulator employing ridge structure, IEEE Photon Technol Lett 5 (1993), 52–54.
6. K. Noguchi, O. Mitomi, H. Miyazawa, and S. Seki, A broadband Ti:$LiNbO_3$ optical modulator with a ridge structure, J Lightwave Technol 13 (1995), 1164–1168.
7. F. Laurell, J. Webjörn, G. Arvidsson, and J. Holmberg, Wet etching of proton-exchanged lithium niobate—A novel processing technique, J Lightwave Technol 10 (1992), 1606–1609.
8. H.J. Lee and S.Y. Shin, Lithium niobate ridge waveguides fabricated by wet etching, Electron Lett 31 (1995), 268–269.
9. W.L. Chen, R.S. Cheng, J.H. Lee, and W.S. Wang, Lithium niobate ridge waveguides by nickel diffusion and proton-exchanged wet etching, IEEE Photon Technol Lett 7 (1995), 1318–1320.
10. R.S. Cheng, W.L. Cheng, and W.S. Wang, Mach-Zehnder modulators with lithium niobate ridge waveguides fabricated by proton-exchange wet etch and nickel indiffusion, IEEE Photon Technol Lett 7 (1995), 1282–1284.
11. R.S. Cheng, T.J. Wang, and W.S. Wang, Wet-etched ridge waveguides in Y-cut lithium niobate, J Lightwave Technol 15 (1997), 1880–1887.
12. Y.P. Liao, D.R. Chen, R.C. Lu, and W.S. Wang, Nickel-diffused lithium niobate optical waveguide with process-dependent polarization, IEEE Photon Technol Lett 8 (1996), 548–550.
13. P.K. Wei and W.S. Wang, Fabrication of lithium niobate optical channel waveguides by nickel indiffusion, Microwave Opt Technol Lett 7 (1994), 219–221.

CCC 0895-2477/99

A METHOD FOR FDTD COMPUTATION OF FIELD VALUES AT SPHERICAL COORDINATE SINGULARITY POINTS APPLIED TO ANTENNAS

Gang Liu,[1] Craig A. Grimes,[1] and Keat Ghee Ong[1]
[1] Department of Electrical Engineering
University of Kentucky
Lexington, Kentucky 40506-0046

Received 11 August 1998

ABSTRACT: *A method is presented for the computation of field values at the singularity points associated with FDTD solution of Maxwell's equations in spherical coordinates; the described numerical technique allows for a complete field solution over the entire computational space including the poles and origin.* © 1999 John Wiley & Sons, Inc. Microwave Opt Technol Lett 20: 367–369, 1999.

Key words: *FDTD; antenna; scattering*

1. INTRODUCTION

The finite-difference time domain, FDTD, a widely used and useful numerical technique for solving Maxwell's equations, cannot be easily applied to problems supporting spherical geometry since there are numerical singularities associated with the poles and origin [1]. For example, the electric field components E_ϕ approach infinity at the origin, and are undefined at the North and South Poles. In this paper, we present a three-dimensional FDTD algorithm to solve for the field values directly, over the total computational space including the origin and poles.

The computational space is divided into three zones: the singularity zone where the poles and origin are located, a one-cell-deep buffer zone that surrounds the singularity zone, and the natural spherical grid zone where the spherical grid can be used without concern. In the singularity zone, the basic spherical FDTD grids are not constructed; rather, a Cartesian grid is used. In the buffer zone, both a spherical grid and a Cartesian grid are established, and in the remaining area, the spherical grid zone, spherical FDTD grids are used exclusively.

All field components in the spherical grid zone and buffer zone are first calculated from the basic spherical FDTD grids [1]. The field values in the buffer zone are then mapped from spherical to Cartesian coordinates using quadratic spatial interpolation to match to the rectangular grid points in the buffer region. A second-order wave equation in Cartesian space is then constructed, which is applicable to a small volume surrounding the singularity point; the volume boundary is in the buffer zone, where the Cartesian grid field values have been obtained. The wave equation is then discretized using a special difference technique so as to obtain a new second-order finite-difference equation. This new equation includes one unknown quantity which is the Cartesian coordinate field value(s) at the spherical grid singularity point, and several known quantities which are the field values of the buffer zone rectangular grid points. We determine the field values of a singularity point by solving this new equation in Cartesian space where numerical singularities associated with the poles and origin do not exist, then transform the field values from Cartesian coordinates to spherical coordinates. Repeating the above procedure, we can obtain all field values for the spherical grid points in the singularity zone, allowing for determination of each spherical field component in the total computational space.

2. PROCEDURE

Assuming a linear, homogeneous, isotropic, and source-free region surrounding the singularity zone, we have an electric field wave equation of the form

$$\nabla^2 \mathbf{E} - \frac{1}{c^2}\frac{\partial^2 \mathbf{E}}{\partial t^2} = 0 \qquad (1)$$

where c is the velocity of light.

The problem space is a small volume which includes the singularity point. For example, consider coordinate point

$E_0(0, 0, z_0)$ as shown in Figure 1. In the vicinity of point E_0, the electric field component E is taken to be a linear function of z along the z-axis. Expanding Eq. (1) in Cartesian coordinates,

$$\frac{\partial^2 E}{\partial x^2} + \frac{\partial^2 E}{\partial y^2} - \frac{1}{c^2}\frac{\partial^2 E}{\partial t^2} = 0. \tag{2}$$

Next, we consider a plane passing through the problem space at singularity point E_0 in parallel with the XY-plane, as shown in Figure 1; there is only a single spherical coordinate point on this plane, at $z = z_0$. Applying the second-order finite-difference expressions to the region surrounding the space point E_0, Eq. (2) can be rewritten as

$$\begin{aligned} &E^{n+1}(0,0,z_0) \\ &\quad = 2E^n(0,0,z_0) - E^{n-1}(0,0,z_0) \\ &\quad + c^2\Delta t^2\left[\frac{E^n(\Delta x,0,z_0) + E^n(-\Delta x,0,z_0) - 2E^n(0,0,z_0)}{\Delta x^2}\right] \\ &\quad + c^2\Delta t^2\left[\frac{E^n(0,\Delta y,z_0) + E^n(0,-\Delta y,z_0) - 2E^n(0,0,z_0)}{\Delta y^2}\right] \end{aligned} \tag{3}$$

where n indicates the time increment, Δx and Δy are the spatial increments of the finite-difference grid in the Cartesian coordinate system, and Δt is the time increment of grid. The space points of Eq. (3) are shown in Figure 1.

Knowing the field values at space points E_1 through E_4, field values at point E_0 can be obtained from Eq. (3). The field components of space points E_1 through E_4 are in Cartesian coordinates, which may, but probably do not, overlap spherical grid points, as shown in Figure 1. Hence, the Cartesian field components of space points E_1 through E_4 in the buffer zone are obtained by a quadratic interpolation of the fields at the surrounding natural spherical grid points, for which the field components are obtained from the basic spherical FDTD grids [1]. Substituting these known field values into Eq. (3), we can then find the field values of Cartesian point E_0, which are then transformed back to spherical coordinates. Repeating the above procedure, we can calculate all field components at any point in the spherical grid, including the origin and z-axis. The magnetic field values in spherical coordinates H_r, H_θ, and H_ϕ for any point in the singularity zone can be calculated using the same procedure.

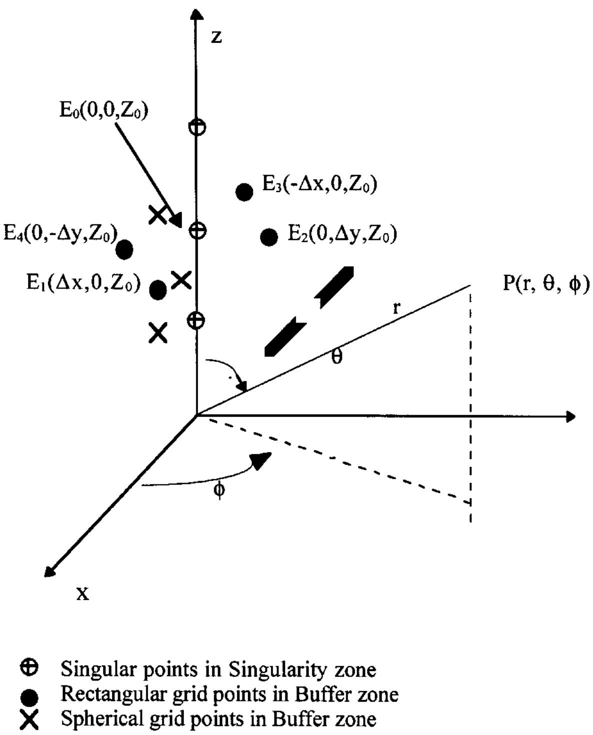

Figure 1 Coordinates and schematic drawing of grid points in singularity and buffer zones

3. RESULTS

The described procedure is used to calculate E_ϕ of a radially oriented electric dipole offset from the origin, shown in Figure 1, along the z-axis. Our FDTD computational space is a sphere 20 cm in radius, with cell dimensions $\Delta r = 5$ mm, $\Delta\theta = \Delta\phi = 7.5°$, so $N_r = 30$, $N_\theta = 25$, and $N_\phi = 49$. The frequency $f = 1.2$ GHz. The time step $\Delta t = 0.14$ ps is sufficient to satisfy Courant's stability criterion. The dipole length is $5\Delta r$, and the wire radius is $0.2\Delta r$. The excitation is a radially directed voltage source ramped to steady-state values [2]; the excitation source cell of the dipole antenna is at ($5\Delta r$, $6\Delta\theta$, $6\Delta\phi$). Since the wire radius is smaller than the cell dimensions, a subcellular thin wire technique [3, 4] was used to include effects of the wire on the update equations. A first-order radiation boundary condition in spherical coordinates was used [5].

To verify our FDTD calculations, the steady-state time-domain fields are converted to the frequency domain by a Fourier transform, and the results are compared to those obtained using NEC4 MoM. Figure 2 shows a comparison of the E_ϕ radiation field along the z-axis for the electric dipole antenna of Figure 1; the results demonstrate the validity of our new approach.

4. CONCLUSIONS

Numerical solutions using FDTD become unbounded and undefined when working in spherical coordinates at grid points along the z-axis, defined by the line $\theta = 0$ to $\theta = \pi$.

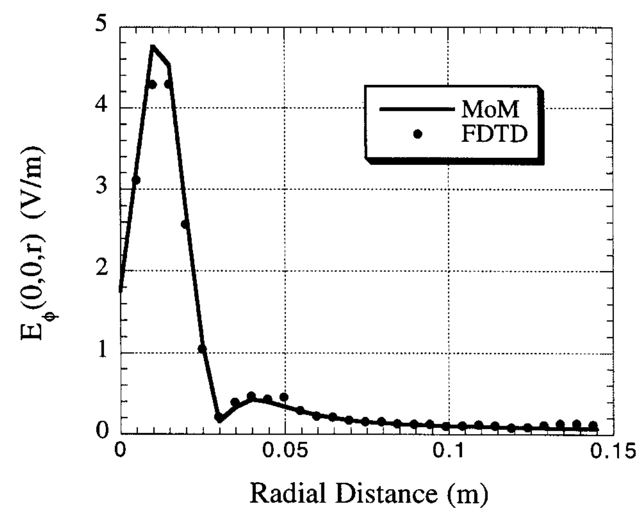

Figure 2 E_ϕ of radially directed electric dipole offset from the origin as a function of distance along the $+z$-axis calculated using FDTD and MoM

The method we have described here is successful in removing all singularities from the FDTD approximations of Maxwell's equation on spherical grids. In our procedure, the total computational space is divided into three regions: the singularity zone in which a Cartesian grid is used, the buffer zone in which both spherical and Cartesian grids are used, and the spherical grid zone. Using the standard spherical FDTD algorithm [1], we solve for the fields at spherical grid points in the spherical zone and buffer zone. In the buffer zone, we interpolate from the spherical grid points to determine field values at near-neighbor rectangular points. Working then in Cartesian coordinates, field solutions are then obtained for the singularity points by solving the second-order wave equation with known boundary conditions. Finally, field values can then be transformed from Cartesian coordinates to the spherical grid, and the solution is complete.

The model is an important extension of the FDTD spherical algorithm [1], allowing for a complete field solution of the entire computational space including the poles and origin. Further, the described solution technique may be extended to other curvilinear coordinates.

ACKNOWLEDGMENT

The authors gratefully acknowledge the support of this work by the U.S. Air Force Office of Scientific Research under Contract F49620-96-1-0353.

REFERENCES

1. R. Holland, THREDS: A finite-difference time-domain EMP code in 3D spherical coordinates, IEEE Trans Nucl Sci 30 (1983), 4592–4595.
2. G. Liu, C.A. Grimes, K.G. Ong, and D.M. Grimes, Time and frequency domain numerical modeling of outbound and standing power from perpendicularly oriented, electrically small TM dipoles, Rev Progress in Applied Computational Electromagn, Proc, 1998, pp. 194–203.
3. K.S. Kunz and R.J. Luebbers, The finite difference time domain method for electromagnetics, CRC Press, Boca Raton, FL, 1993.
4. A. Taflove, Computational electrodynamics: The finite-difference time-domain method, Artech House, Norwood, MA, 1995.
5. A. Bayliss and E. Turkel, Radiation boundary conditions for the wave-like equations, Commun Pure Appl Math 33 (1980), 707–725.

THE STUDY OF AN ELECTROMAGNETIC SCATTERING MODEL FOR TWO ADJACENT TRUNKS ABOVE A ROUGH SURFACE GROUND PLANE

Wang Xiande,[1] Luo Xianyun,[1] Zhang Zhongzhi,[1] and Fu Junmei[2]
[1] China Research Institute of Radiowave Propagation
XingXiang, Henan 453003, P.R. China
[2] Xi'an Jiaotong University
Xi'an 710049, P.R. China

Received 15 August 1998; revised 14 October 1998

ABSTRACT: *In this paper, the finite-length multilayer dielectric cylinder is used to model a trunk, and the electromagnetic scattering model for two adjacent trunks above a rough surface ground plane is analyzed by using the reciprocity theorem. The scattering amplitudes including the second-order scattering terms are given. The influence of the bark layer on the scattering pattern is discussed at L-band, C-band and X-band.* © 1999 John Wiley & Sons, Inc. Microwave Opt Technol Lett 20: 369–376, 1999.

Key words: *electromagnetic scattering; finite-length multilayer dielectric cylinder; reciprocity theorem*

1. INTRODUCTION

Because the forest ecosystems represent a significant portion of the earth's vegetation, and play an important role in the global carbon cycle, the development of scattering models that accurately simulate backscattering from such canopies is very important. During the past few years, several models have been developed for predicting microwave backscatter from forested areas, such as MIMICS1 (Michigan Microwave Canopy Scattering model) developed by Ulaby et al. [1], MIMICS2 (for discontinuous tree canopies) developed by McDonald and Ulaby [2], and the multiconstituent and multilayer model developed by Chuah [3]. In these models, forest canopies have been considered as consisting of a crown layer (which may consist of more than one layer), a trunk layer, and ground surface. These models, based on the radiative transfer model or Monte Carlo technique for calculating the backscatter cross section from forest canopies, suppose that discrete scatter particles are located in regions far from each other using the single scattering characteristic. When the number densities of the scatterers become large enough, the interaction of adjacent scatterers must be considered. In these models, the trunk is modeled as a single-layer dielectric cylinder, while using a finite-length multilayer dielectric cylinder modeling the natural trunk is more reasonable. So, in this paper, the trunk is modeled as a finite-length multilayer dielectric cylinder. The scattering amplitude matrix of the multilayer dielectric cylinder is calculated using the iterative algorithm [4], and the scattering cross section of two adjacent trunks above the rough surface is calculated by using the reciprocity theorem [5]. Numerical examples are demonstrated, and the results of the influence of the bark layer on the scattering cross section have been discussed at L-band, C-band and X-band.

2. THEORETICAL FORMULATIONS

2.1. Scattering from Infinite Radially Dielectric Cylinder. The determination of the scattering response of an infinite radially layered circular cylinder is the object of the present section. Each individual layer is characterized by different electromagnetic properties. The iterative algorithm is described in [4]. The radii of the K concentric layers of the cylinder are defined by $a^k(k = 1,2,\ldots,K)$. Layer $K+1$ corresponds to the zone outside the cylinder. The electromagnetic properties can be characterized by ε_k and μ_k ($k = 1,2,\ldots,K$), respectively, if $k = K+1$, ε_k, and μ_k are equal to 1 respectively. The unit vector $\hat{k}_i$ of the incident plane wave forms an angle of θ_i with the z-axis and ϕ_i with the x-axis, respectively. It is decomposed into TM and TE components, which produce the following z-components of electric and magnetic fields:

$$E_z^i(\rho, \phi) = E_0 \sin\theta_i e^{-j\beta_\rho^{K+1}\rho\cos(\phi-\phi_i)} e^{-j\beta_z^{K+1}z} \tag{1}$$

$$H_z^i(\rho, \phi) = H_0 \sin\theta_i e^{-j\beta_\rho^{K+1}\rho\cos(\phi-\phi_i)} e^{-j\beta_z^{K+1}z} \tag{2}$$

where $\beta_\rho^K = 2\pi/\lambda_0$, and λ_0 is the wavelength of the incident plane wave. Using the well-known addition theorem for Bessel functions, the incident field can be expressed as a series of